Multifunctional Biodegradable Polyacrylamide Nanocarriers for Cancer Theranostics—A "See and Treat" Strategy

Shouyan Wang,[†,§] Gwangseong Kim,[†] Yong-Eun Koo Lee,[†] Hoe Jin Hah,[†] Manivannan Ethirajan,[‡] Ravindra K. Pandey,[‡] and Raoul Kopelman[†,*]

[†]Department of Chemistry, University of Michigan, Ann Arbor, Michigan 48109, United States and [‡]PDT center, Roswell Park Cancer Institute, Buffalo, New York 14263, United States. [§]Present address: EaglePicher Technologies LLC, 3220 Industrial Drive, Joplin, Missouri 64801.

ABSTRACT We describe here the development of multifunctional nanocarriers, based on amine-functionalized biodegradable polyacrylamide nanoparticles (NPs), for cancer theranostics, including active tumor targeting, fluorescence imaging, and photodynamic therapy. The structural design involves adding primary amino groups and biodegradable cross-linkers during the NP polymerization, while incorporating photodynamic and fluorescent imaging agents into the NP matrix, and conjugating PEG and tumor-targeting ligands onto the surface of the NPs. The as-synthesized NPs are spherical, with an average diameter of 44 nm. An accelerated biodegradation study, using sodium hydroxide or porcine liver esterase, indicated a hydrogel polymer matrix chain collapse within several days. By using gel permeation chromatography, small molecules were detected, after the degradation. *In vitro* targeting studies on human breast cancer cells indicate that the targeted NPs can be transported efficiently into tumor cells. Incubating the multifunctional nanocarriers into cancer cells enabled strong fluorescence imaging. Irradiation of the photosensitizing drug, incorporated within the NPs, with light of a suitable wavelength, causes significant but selective damage to the impregnated tumor cells, but only inside the illuminated areas. Overall, the potential of polymeric-based NPs as biodegradable, multifunctional nanocarriers, for cancer theranostics, is demonstrated here.

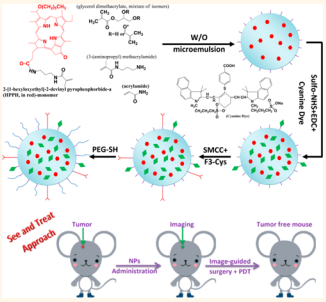

KEYWORDS: polymer · nanoparticle · cancer · photodynamic therapy · imaging · targeting · multifunctional

Current cancer therapy usually involves surgery, so as to remove the tumors, if possible, followed by chemotherapy and/or radiation.[1] When feasible, maximal surgical resection of the tumor may indeed improve survival.[2] But success in surgery still relies on the surgeon's ability to judge the presence of residual tumor tissue at the time of surgery,[3] the reason being that neoplastic tissue, while easily detected radiographically, is virtually indistinguishable from normal brain tissue.[4] For chemotherapy or radiation therapy, the anticancer drugs often fail to kill cancer cells as they are usually administered systemically, and therefore are subject to variations in their absorption, metabolism, and delivery to target tissues.[5] Thus, there is a clear need for improving surgery by tumor delineation during surgery, as well as for an adjuvant treatment that would sterilize the tumor bed, say intraoperatively, with minimal or no side-effects.

Investigators have proposed the use of multiple imaging agents to aid in the recognition of neoplastic tissue during resection.[6−9] The first use of fluorescein, to improve the detection and identification of brain tumors *in vivo,* was reported by Moore *et al.* in 1948.[7] Unfortunately, it is very difficult to implement feasible tumor imaging techniques which simultaneously offer sufficient specificity and sensitivity. Most striking is the recognition that only between 1 and 10 parts per 100 000 of intravenously administered contrast agents reach their parenchymal targets *in vivo*.[9,10] On another front, photodynamic therapy (PDT) has emerged as one of the important therapeutic options in cancer management. PDT is a clinical treatment that utilizes the combined action of photosensitizers (PSs) and specific light sources for the treatment of various cancers. For PDT to be successful, the availability of suitable PSs and an appropriate formulation for high accumulation in the tumor are of crucial importance. It is believed that the vast majority of neoplastic cells are found within the tumor bed and up to 2 cm beyond the enhancing borders.[11] For a 630 nm

* Address correspondence to kopelman@umich.edu.

Received for review April 13, 2012 and accepted June 17, 2012.

Published online June 17, 2012
10.1021/nn301633m

laser light beam (used with Photofrin, the first generation PS), the light penetration depth, into the tumor, ranges from 6 to 12 mm,[10] indicating that, for deep enough penetration, longer activation wavelength PSs, that is, the so-called second generation PSs, may be required for complete tumor killing. However, most second-generation PSs are very hydrophobic and not easy to formulate. Meanwhile, they also lack high selectivity to tumor tissues, which can result in severe side effects when injecting the PS directly.[12] 5-Aminolevulinic acid has been reported to induce selective accumulation of an endogenous PS, protoporphyrin IX, in gliomablastoma multiforme. However, a very high dose (>100 mg/kg) is needed for reliable *in vivo* fluorescence imaging.[13]

Nanotechnology offers a tremendous potential for medical diagnostics and novel therapeutic modalities. There have been explosive developments of nanomedicine platforms over the past decade and the combination of different nanoscale materials can lead to the development of multifunctional medical nanoplatforms for simultaneous targeted delivery, fast diagnosis, and efficient therapy.[14] Various types of NPs have been extensively studied for numerous biomedical applications. Among the many nanoparticulate systems, polymeric NPs have been intensively investigated for their potential application as delivery vehicles for small-molecule drugs,[15−19] DNA,[20,21] and proteins.[22,23] A premise of nanomedicine is that it may be feasible to develop multifunctional constructs combining diagnostic and therapeutic capabilities, thus leading to a better targeting of drugs to diseased cells, as well as better monitoring of the therapeutic process.[24] This is often called "theranostics". Of specific interest is "targeted theranostics".[25]

In view of the above-mentioned facts, we adopted a "see and treat" strategy for tumor treatment, by using biocompatible/biodegradable polymeric NPs. Our previous *in vivo* work using the NPs already evidenced the specific targeting of F3 peptide,[26] image guided tumor resection and therapy,[19] respectively. This is a continuation work to make a better delivery system, that is, less drug leaching after administration, by combining all mentioned advantages together with a different drug loading method. Specifically, the approach of intraoperative visualization, followed by intraoperative therapy, is currently one of the most promising methods for complete eradication of malignant brain tumors.[12,27] As the singlet oxygen, a primary cytotoxic reactive oxygen species ROS, has a lifetime of less than 3.5 μs, and can diffuse only a very short distance (around 120 nm in water, but only 10 to 20 nm *in vivo*[28]), the initial extent of the photodamage is limited to the site of the PS drug molecule. This requires that the designed PDT NPs are made of an oxygen-permeable matrix and have a diameter of less than 200 nm, and reasonable drug loading. The size of the NPs should also be larger than 10 nm, as the tight endothelial junctions of normal blood vessels typically are of 5 to 10 nm in size.[29] The idea described here involves combining such PDT NPs, with fluorescence imaging agents, for simultaneous cancer imaging and delineation. The prepared multifunctional nanocarrier is further modified by adding a tumor-targeting and cell penetrating peptide, which seeks out and enters cancerous cells, as well as by adding PEGylation, so as to prolong the blood circulation time. By taking advantage of both the imaging and PDT agents, this novel nanomedicine is expected to improve the ability of surgeons to achieve maximal resection of tumors, with the help of fluorescence guided tumor margin delineation, enhanced further by photodynamic therapy to be performed after the tumor resection, for the removal of any tumor tissues left behind. Herein, we report a novel protocol for the preparation of such a multifunctional nanomedicine, as well as the characterization needed so as to evaluate the toxicity, sensitivity, and biodegradability of the prepared nanomedicine. Furthermore, we report on an *in vitro* investigation of the targeted detection ability of the nanocarrier, and on its synergistic tumoricidal efficacy on brain and breast tumor cells.

RESULTS AND DISCUSSION

The synthetic procedure of the multifunctional polymer nanomedicine is presented in Figure 1a. Amine-functionalized polyacrylamide (AFPAA) PS conjugated NPs were prepared by using a modified water-in-oil microemulsion method.[30] The PS, 2-devinyl-2-(1-hexyloxyethyl) pyropheophorbide (HPPH), which is very hydrophobic and currently in phase II human clinical trials, shows large molar extinction coefficient in the red region of the visible spectrum (660 nm), a high singlet oxygen quantum yield of 0.48, and only mild skin photosensitivity and has elicited in patients considerably less potential for cutaneous phototoxicity than for patients receiving Photofrin or Foscan.[31] It has been synthesized and modified to an HPPH-conjugated acrylamide derivative at Roswell Park Cancer Institute (see Figure 1 for structures of HPPH and HPPH-conjugated acrylamide[32]). After polymerization with other monomers, HPPH becomes a part of the nanohydrogel matrix, which makes the nanomedicine easier to formulate, because of the higher solubility of the hydrogel in aqueous solution, as demonstrated below. Most importantly, the conjugated PSs are not released after being administrated, as they are restrained to the nanomedicine matrix region, which is beneficial with respect to side effects reduction that HPPH by itself may cause, and thus also enables a higher dose usage. Conjugation of the cyanine dye (CD, see Figure 1 for reaction schematics) to the NP (both its surface and inside the matrix) was performed, based on standard procedures,[33] by taking advantage of the primary

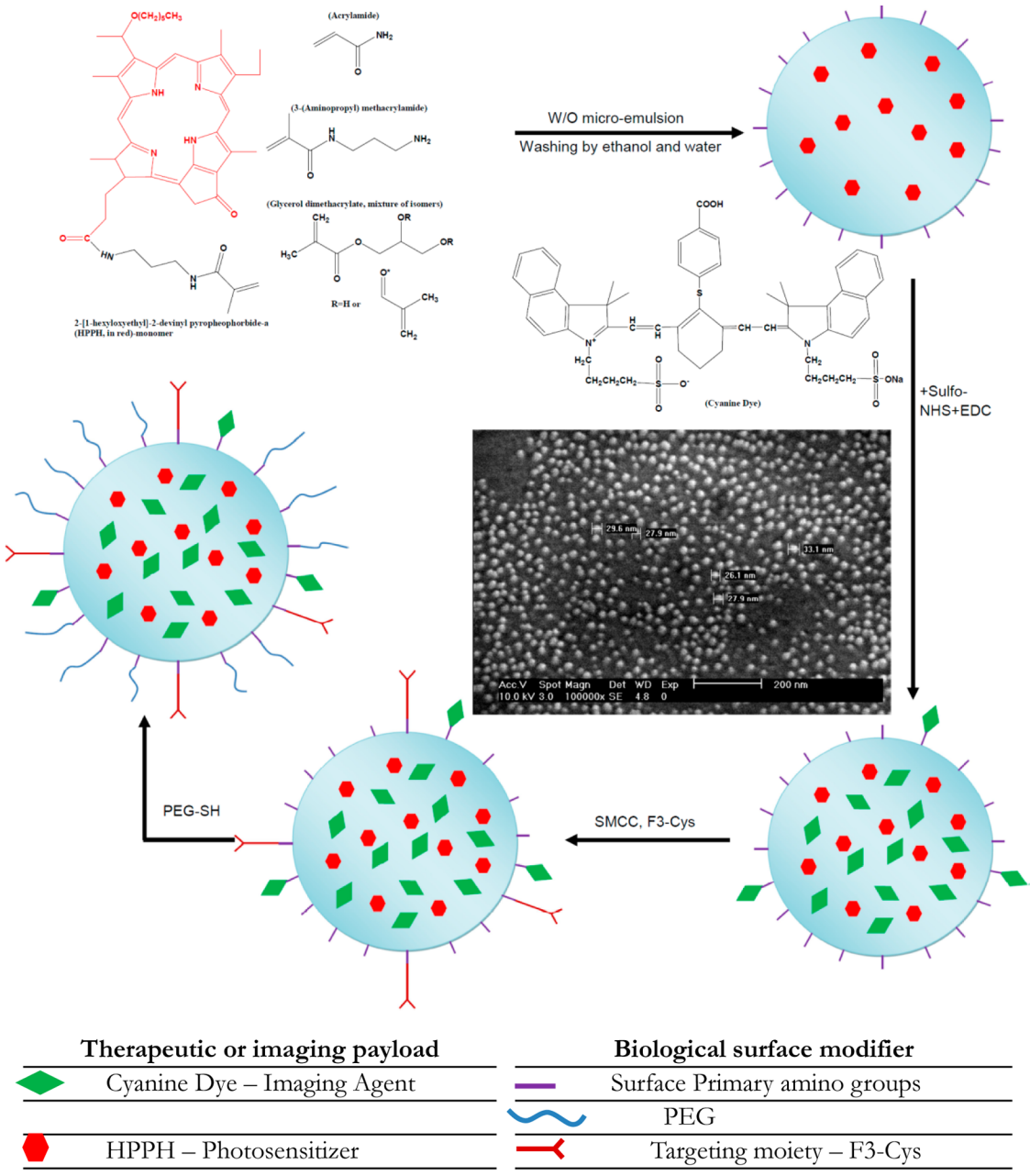

Figure 1. Synthetic procedure for the multifunctional polymer nanomedicines.

amino groups in the NP polymer chains and a carboxyl group in the cyanine dye. Poly(ethylene glycol) (PEG) was used to modify the surface of the NP, so as to prolong blood retention time.[34−38] The typical morphology of the as-prepared NPs is shown in the inset of Figure 1. The average size of the NPs is around 44 nm, based on the results from dynamic light scattering (DLS). This larger size derived from DLS, compared to that measured from SEM (28 nm, averagely) can be ascribed to the swelling of the hydrogel at aqueous conditions.[39−41] The payloads for the HPPH and CD were calculated, based on absorption measurements, to be 0.69 and 1.47 wt %, respectively. Thus the numbers of PS and imaging agent molecules for each NP were determined to be 75 and 98 per NP, respectively. The number of targeting moieties was 8 per NP, based on quantitative amino acid analysis (QAAA). Dye leaching test results by using ethanol indicated that no HPPH leached out, but 4% of CD in all filtrates collected did. The leached out CD indicates that some of the CD dye molecules were not conjugated but adsorbed onto the NP matrix during the postconjugation process.[32]

Most of the degradable and biodegradable polymers contain hydrolyzable linkages, such as ester, ortho-ester, and anhydride, in their backbones.[42] Figure 2a shows the structure of the blank AFPAA NPs designed. The degradation of AFPAA NPs is considered to be a hydrolytic progress in which the cleavage of an

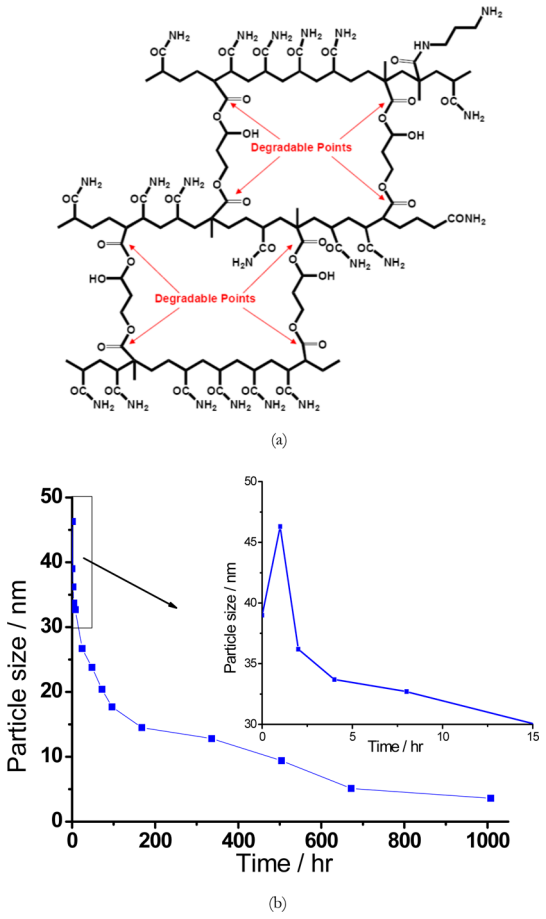

Figure 2. Degradation study of AFPAA NPs: (a) structure of blank AFPAA matrix designed, where the degradation points are shown by arrows; (b) particle size *vs* time relationship of AFPAA NPs in 1 M sodium hydroxide solution at room temperature.

ester group yields a carboxyl end-group and a hydroxyl one, just like for other polyesters. Figure 2b shows the particle size *versus* time relationship in a 1 M sodium hydroxide solution. For accelerated NP hydrolysis, it can be seen clearly that the particle size increases from 39.4 nm (Supporting Information, Figure 1) to 46.3 nm during the first hour, and then starts to decrease, indicating that the particle matrix chains start collapsing. The observed changes in the particle size can be ascribed to the hydrolysis of the hydrogel that occurs when the nucleophile (*i.e.*, hydroxyl ion) attacks the carbon of the carbonyl group of the ester. In an aqueous base, hydroxyl ions are better nucleophiles than dipolar species such as water. The hydrolysis products are compounds containing carboxyl groups (acids or salts). As carboxyl groups increase the solubility of the AFPAA NPs, as well as the repulsion between the negatively charged carboxyl groups produced, the hydrogels swell more which causes the initial size increase. As the hydrolysis of the esters proceeds, more ester linkages of the matrix break down, causing rapid particle size decrease during the first several days, as shown in Figure 2b. As the sodium hydroxide was neutralized by the biodegradation products gradually, the degradation speed decreased gradually over longer periods. After four weeks, the average size of the hydrogel was already reduced to less than 5 nm. While, in 1 mg/mL porcine liver esterase, similar processes were observed, but without swelling, as esterase cannot convert ester groups to carboxyl groups the way sodium hydroxide did. Gel permeation chromatography (GPC) results confirmed that small molecular species were produced after hydrolysis. Smaller biodegradation products can enter the pores of the GPC column more easily, and therefore spend more time in these pores, thereby increasing their retention time. Conversely, larger polymeric products spend little time in the pores and are eluted quickly. The molecular weights of the degradation products were calculated on the basis of standard curves obtained by using the retention time of polyacrylamide standards. After 4 days in porcine liver esterase aqueous solution, the degradation products had molecular weights of 1142 Da and 549 Da, indicating that the degradation process was not homogeneous. Also, there were some big pieces detected showing molecular weights around 500 KDa. Using sodium hydroxide did accelerate the degradation process significantly; the calculated molecular weight was 522 Da and 296 Da after 1 week storage in 1 M NaOH at 37 °C, indicating that the NP matrix had totally collapsed into shorter polymer fragments.

Surface modification of pharmaceutical nanocarriers is normally used to control their pharmacokinetic behaviors in a desirable fashion while the nanocarriers perform various therapeutic or diagnostic functions.[35,43] Our modified nanohydrogels have attached PEG chains and F3 peptides, which is confirmed by QAAA results and by a slightly positive surface charge (+9 mV, by zeta potential). The size of the nanocarriers after modification is around 44 nm (by dynamic light scattering), which enables the NPs to obtain a greater ability to target the site of interest.[1] Sterically stabilized nanocarriers, by the PEG corona, have shown prolonged blood circulation through avoidance of removal by the reticuloendothelial systems (RES), which thus enhanced "passive" targeting to solid tumors through the enhanced permeability and retention effect, as NPs can penetrate through small capillaries and are taken up by cells, which allows for efficient drug accumulation.[44] Although the leaky vasculature of solid tumors enhances accumulation in tumor tissues, significant NP uptake in the RES, such as liver and spleen, has also been observed. To further improve delivery, efficiency, and cancer specificity, a strong impetus has been placed on the development of nanoparticulate systems that can actively target tumors through molecular recognition of unique cancer-specific markers. The F3 peptide, a 31-amino acid synthetic peptide derived from a fragment of the high mobility group protein 2, has been used as a tumor targeting marker for cancer treatment.[34,45] Tissue and cellular localization

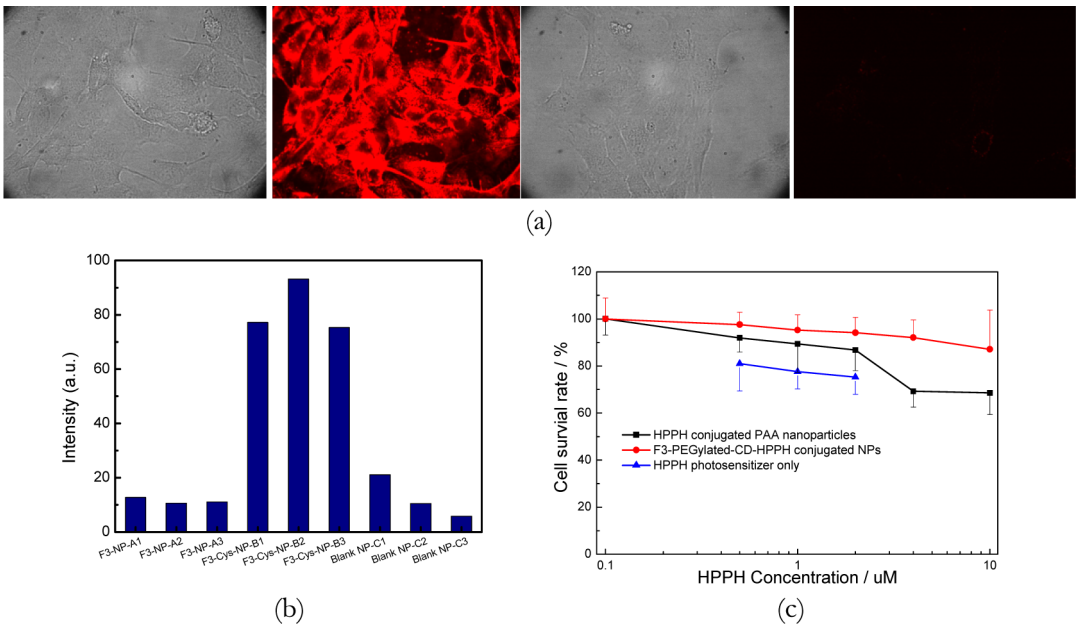

Figure 3. (a) Confocal images showing the target-specificity of F3-Cys peptide in 9 L Glioma tumor cells. These results illustrated the target-specificity of F3-Cys containing PEGylated rhodamine conjugated AFPAA NPs (left two: bright field image and fluorescence image of rhodamine), in contrast to the corresponding nontargeted analog (right two: bright field image and fluorescence image of rhodamine). The cells were incubated with NPs for 15 min and washed three times to remove unbound NPs. (b) Fluorescence intensity of cells targeted by F3, F3-Cys, and nontargeted NPs in nucleolin rich MDA-MB-435 cancer cell. (c) MTT assay of HPPH PSs and surface modified AFPAA NPs (triangle, HPPH only; square, HPPH conjugated AFPAA NPs without surface modification; circle, F3-Cys targeted PEGylated CD linked HPPH conjugated AFPAA NPs. HPPH concentration is 10 μM in 1 mg/mL NPs suspension). Note: These are "dark toxicity" tests.

TABLE 1. QAAA Results for Targeting Optimization Using Different Amounts (Indicated as 1, 2, and 3) of Surface Modification Moieties ((A) F3; (B) F3-Cys; and (C) cysteine)

expt no.	(A) F3 amount, μg	(B) F3-Cys amount, μg	(C) cysteine amount, μg
1	2.6	2.7	0.29
2	5.1	5.3	0.58
3	7.7	8.0	0.87

of the F3 peptide indicated that this peptide homes selectively onto tumor blood vessels (angiogenous vasculature) and tumor cells and has the remarkable property of being able to carry a payload into the cytoplasm and even nucleus of the target cells.[45] Thus the attractive property of the F3 peptide is that it is internalized into its specific target cells.[34] The targeting efficiency of our F3 guided nanomedicine was investigated by using fluorescent NPs prepared with the same AFPAA NPs but containing covalently linked rhodamine dye and having approximately the same size and surface charge as the HPPH containing nanomedicine for two nucleolin overexpressing cell lines, the MDA-MB-435 breast cancer cell line and the 9 L human glioma cell line.[3] To evaluate the targeting efficiency, the PEGylated NPs without F3 attachment were prepared as a reference. Figure 3a shows the *in vitro* targeting experimental results for the NPs with optimized amounts of F3 peptide. The strong fluorescence spectra of the rhodamine indicated that the F3 targeted AFPAA NPs were bound/internalized to/by the cells just after 15 min incubation, while there was no rhodamine fluorescence detectable from the cells treated with NPs without the F3 attachment, not even after 4 h incubation. The optimized amount of F3 was determined by measuring the fluorescence intensity of cells incubated by NPs with different amounts of the F3-Cys attached. It can be seen from Figure 3b and Table 1 that the F3-Cys gave a much higher targeting efficiency than the F3 peptide. It also shows that No.2 NPs with F3-Cys capped (Table 1, B2) have the highest targeting efficiency, although the F3-Cys amounts were less than for No.3 NPs (*i.e.*, B3).

For the living cell study, the next thing investigated was the dark toxicity of HPPH conjugated NPs without/with surface modification. Stock NP solutions of HPPH conjugated AFPAA NPs and F3-Cys targeted PEGylated CD linked HPPH conjugated AFPAA NPs were made in PBS buffer saline, respectively, to prepare a series of different dye containing solutions. After incubation for 3 h, in incubator, MDA-MB-435 cells were washed with fresh DMEM buffer three times, so as to remove any residue NPs, and cell viabilities, after treatment with NPs, were quantified by an MTT assay (Figure 3c). It can be seen that the toxicity of the PS-conjugated NPs increases gradually with the HPPH concentration (thus the NP concentration), especially at concentrations higher than 2 μM. As demonstrated before, AFPAA NPs are not toxic at all[30,46–49] for *in vitro* experiments, even at higher concentrations (5 mg/mL). Thus, comparing all

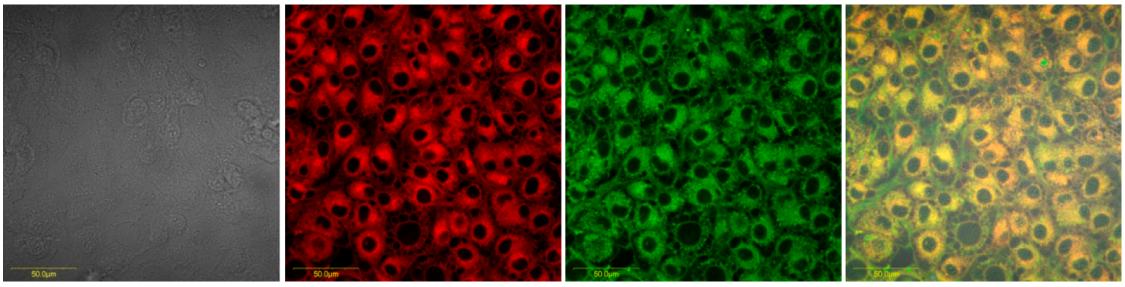

Figure 4. Confocal image of F3-Cys targeted PEGylated FITC linked HPPH conjugated AFPAA NPs (from left to right: bright field cell image; HPPH binding image; FITC binding image; and combining all images together).

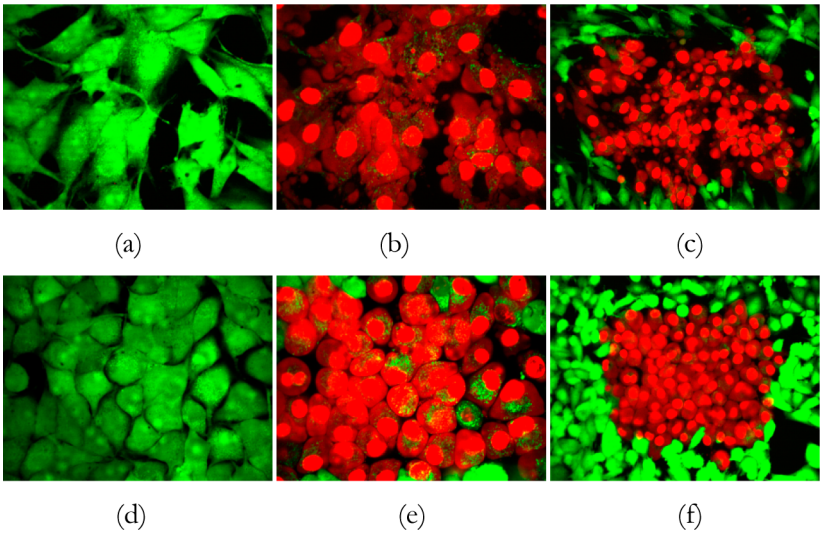

Figure 5. Images of 9 L (upper row) and MDA-MB-435 (lower row) tumor cells treated with F3-Cys targeted PEGylated CD linked HPPH conjugated AFPAA NPs with 1 μM HPPH concentration, illuminated with 647 nm laser light (46 uW) for 1 min, and monitored every minute thereafter. 9 L: (a) 0 min (40× magnification); (b) 15 min; (c) 20× zoom out image. MDA-MB-435: (d) 0 min (40× magnification); (e) 15 min; (f) 20× zoom out image.

results at the same concentration, it is the HPPH PS itself that can be correlated with cell death, indicating that some of the conjugated HPPH may stay close to or on the surface of the NPs. For nanocarriers with surface modification (PEG + F3-Cys), the dark toxicity was found to be suppressed a lot, especially for the higher dye loading amounts. These results are promising; as demonstrated before, the targeted NPs are prone to accumulate more in the cells compared with nontargeted ones for the same incubation time. That is, even though there are more nanomedicines (nanocarriers), that is more PSs, in each cell, because of the higher cellular uptake of the targeted NPs, the toxicity of the carriers is not increased, but rather decreased, because of the PEG/F3-cys peptide corona. As there is no near-IR camera available, CD was replaced by FITC for the following *in vitro* experiments as the final modified NPs have the same size and surface charge. Figure 4 shows the fluorescence images of impregnated MDA-MB-435 breast cancer cells after 15 min incubation with F3-Cys targeted, PEGylated, FITC linked, HPPH conjugated, AFPAA NPs. It clearly shows a strong intensity for both fluorophores loaded. The overlapped image shows more than 90% in yellowish color (Adobe Creative Suite CS4) indicating there is no leaking after NPs uptake and these two fluorophore do not affect each other.

The PDT effectivity is largely determined by the intactness of the drug itself,[50,51] the drug's efficiency of singlet oxygen production and the degree of efficiency and selectivity at which the therapeutic PS is delivered to the target site through delivery vehicle. The calculated singlet oxygen produced to be 2.14×10^{-4}/s (Supporting Information, Figure 2), which is very close to the HPPH itself at the same dye concentration indicating that the linking of targeting and imaging agents does not affect the singlet oxygen production. Our HPPH containing AFPAA nanomedicine did not kill cells when incubated in the dark. However, both 9 L human glioma and MDA-MB-435 breast cancer cells were effectively killed by exposure to 647-nm light (Figure 5). The results indicate that these HPPH-containing NPs cause significant cellular damage in the presence of light. The NPs, even at a very low concentration (1 μM), in combination with light, result in

significant damage to the cells. That is, there are no cells alive in the illumination area, while all the other cells are alive without illumination. Finally, no dark toxicity can be seen over the time span of the experiment, which is longer than 4 h.

CONCLUSION

In summary, we have designed multifunctional biodegradable polyacrylamide nanoplatforms for a "see and treat" strategy, by a combination of photodynamic therapy and fluorescence imaging, for an interesting possibility of cancer theranostics. Modification of the nanoplatform with PEG and tumor targeting cell penetrating peptide enabled guiding the particles to specifically targeted cancer cells and significantly reduced the dark toxicity of the PSs conjugated to/into the nanocarrier. An accelerated biodegradation study, in sodium hydroxide or porcine liver esterase, demonstrated the biodegradability of these polyacrylamide nanomaterials in these aqueous solutions. Multifunctional NPs containing both fluorophores and PS drugs, as well as tumor-targeting moieties, did give bright fluorescence images of specific tumor cells and also generated singlet oxygen, only upon light irradiation, resulting in an irreversible but selective destruction of the cancer cells investigated. Specifically, no interference was found among the multifunctionalities of the nanoplatforms: (1) photodynamic activity, (2) fluorescence imaging, (3) targetability, (4) biodegradability. Furthermore, the nontoxicity, in the dark, is preserved.

METHODS

HPPH Conjugated Amine Functionalized Polyacrylamide NPs Polymerization. Hexane (45 mL; all chemicals obtained from Sigma Aldrich unless otherwise stated) was added into a dried 100 mL round-bottom flask and stirred under a constant purge of argon. Dioctyl sulfosuccinate (1.6 g) and Brij 30 (3.1 g) were added to the reaction flask and stirring was continued under argon protection. In the mean time, acrylamide (0.711 g) and 3-(aminopropyl) methacrylamide (0.055 g) were dissolved in phosphate buffer saline (PBS, pH = 7.4) in a glass vial and 4 mg of HPPH-conjugated acrylamide derivative was dissolved in glycerol dimethacrylate (0.537 g) by sonication for 15 min. The latter mixture was added to the acrylamide solution, and the reaction mixture was sonicated for 5 more minutes to obtain a uniform solution. The solution was then added to the hexane reaction mixture and vigorously stirred for 20 min at room temperature under argon protection. Polymerization reaction was initiated by adding freshly prepared ammonium persulfate (50% aqueous solution, 100 μL) and *N*,*N*,*N*′,*N*′-tetraethylmethylenediamine (100 μL), and the resulting solution was stirred vigorously at room temperature for 2 h. At the completion of polymerization, hexane was removed by rotary evaporation, and the particles were precipitated by the addition of ethanol (Fisher Scientific). The surfactant and unreacted monomers were washed away from the particles with ethanol (5 $\times$ 160 mL) followed by washing with water (5 $\times$ 100 mL) in an Amicon stirred cell (200 mL, equipped with a Biomax 500 kDa cutoff membrane). The concentrated NPs were lyophilized for 2 days before use. The particles were also sized by using dynamic light scattering (DLS, Delsa Nano C), and a scanning electron microscope (SEM, Philips ESEM XL30) was also used to investigate the size and morphology of all the NPs obtained.

Rhodamine-Conjugated AFPAA NPs. The same recipe as previously described for blank NPs[26,32] was followed to make the rhodamine conjugated NPs except that 10 mg of 5-(and 6-) Carboxy-X-rhodamine, succinimidyl ester (Anaspec, Inc.) was added into the monomer solution and stirred for 1 h at 37 °C before being injected into hexane for polymerization.

FITC Linked HPPH Conjugated AFPAA NPs. The same recipe as previously described was followed to make the FITC (Invitrogen, Inc.) linked NPs except that the blank NPs were replaced by the HPPH conjugated ones.[26]

CD-Linked HPPH Conjugated NPs. CD was first modified by taking advantage of its carboxyl groups. *N*-Hydroxysulfosuccinimide (Sulfo-NHS, Thermo Scientific) is used to increase the efficiency of EDC-mediated coupling reactions.[52,53] Specifically, 1 mg of CD was dissolved in MES buffer (pH 6.0), followed by adding 10 mg of 1-ethyl-3-(3-dimethylaminopropyl) carbodiimide hydrochloride (EDC) and 30 mg of Sulfo-NHS. After 15 min reaction, the resultant product was added into HPPH conjugated AFPAA NPs in PBS saline under stirring. Sodium hydroxide aqueous solution (1 M) was used to adjust the pH value to 7.0 or above to initiate the reaction between amine group and *O*-acylisourea. After the reaction was completed, the excess dye was removed from the suspension through an Amicon stirred cell equilibrated with a 100 KDa membrane. The resulting bifunctional NPs were then ready for further surface modification.

Surface Modification of Drug-Loaded AFPAA NPs. The remaining terminal amines of the NPs were conjugated with F3-Cys or PEG-SH. This was realized by reaction between amino groups of NPs and sulfosuccinimidyl-4-(*N*-maleimidomethyl) cyclohexane-1-carboxylate (SMCC, Thermo Scientific). F3-Cys (Polypeptide Group) or PEG-SH (Creative PEGWorks) is attached to the NP through a stable thioether bond that is not susceptible to breakage under reducing conditions.[54] For surface modification, we prepared a stock solution of NPs by dissolving 100 mg of NPs in 5 mL of 10 mM PBS buffer at pH 7.4. A 6 mg sample of SMCC was weighed and added directly into the stock NPs suspension, and the mixture was allowed to react for half an hour at room temperature. After the reaction of SMCC with NPs, the excess SMCC was removed by using a Millipore centrifugal tube equipped with a 100 KDa membrane. After washing, different amounts of F3-Cys were then added to the resulting sulfhydryl-reactive NPs, and the mixtures were stirred overnight. PEG-SH was added directly to the final products the next day and allowed two more hours reaction. Unreacted F3-Cys and PEG-SH were removed from the suspension through washing by using the same centrifugal unit.

F3-Cys Amount Optimization. The same method as the above-mentioned one was used for surface modification. Three different molar amounts of cysteine, F3, or F3-Cys were selected based on our previous experiences. The rinsing procedures described above were followed, so as to remove any residues before they were sent out for QAAA analysis.

Characterization. *UV–vis and Fluorescence Spectra.* The amount of CD covalently binding to NPs was controlled through stoichiometry and reaction conditions and then quantified by fluorescence spectroscopy. The emission intensity of a dilute sample of NP-CD at 843 nm was compared to a linear standard prepared using various concentrations of CD. The number of NPs was calculated on the assumption that AFPAA hydrogel has a density which is the same as DI water. The size of the AFPAA NPs was determined by DLS to be 44 nm. Using this information, we determined the mass of one NP to be 1.15×10^{-17} g and that the reaction yielded 98 fluorophores per NP. Similarly, the number of F3 and F3-Cys peptides and HPPH linked to each NP was quantified using QAAA (Laboratory for protein chemistries, Texas A&M university) and UV–vis spectroscopy, respectively. From these analyses, the average number of F3-Cys molecules per NP was determined to be 8, while the number of HPPH per NP is 75.

Targeting Efficiency Measurement. The 9 L cells were maintained in complete Dulbecco's Modified Eagle Medium (DMEM) that consisted of a-MEM with 10% fetal calf serum, L-glutamine,

penicillin, and streptomycin at 37 °C, 5% CO_2, 95% air, and 100% humidity and then seeded in 96-well plates at a density of 5000 cells/well. After overnight incubation at 37 °C the functionalized NPs were added followed by incubation at 37 °C for 15 min. The cells were washed thoroughly for three times by using sterilized DMEM media to remove any untargeted NPs. The cell images were acquired with a Perkin-Elmer Ultra View confocal microscope system equipped with an argon−krypton laser. The intensity of the fluorophore was quantified as previously described.[32]

MTT Assay. MDA cells were maintained in complete DMEM cell media at 37 °C, 5% CO_2, 95% air, and 100% humidity. Cells were seeded in 96-well plates at a density of 5000 cells/well. After overnight incubation at 37 °C the NPs were added at 0.1 mg/mL and incubated at 37 °C for 3 h in the dark. The cells were washed thoroughly by using sterilized DMEM media for three times, followed by adding 35 μL of 5.0 mg/mL solution in PBS of 3-[4,5-dimethylthiazol-2-yl]-2,5- diphenyltetrazoliumbromi (MTT) and 165 μL of cell media. After 4 h the MTT and medium were removed and 200 μL DMSO was added to solubilize the formazan crystals. Absorbances were read on a microtiter plate reader at 550 nm. Each experiment was done with four replicate wells.

Singlet Oxygen Production Measurement. A chemical probe method as described previously[32] was used to check the singlet oxygen production efficiency.

Laser-Induced in Vitro PDT. MDA-MB-435 and 9 L tumor cells were grown as described in the previous section. These cells were plated in 6-well plates in complete media. The next day, PS and drug-loaded NPs were added at variable concentrations, respectively, together with 2 mL of Hanks 1× balanced salt solution containing 10 mM pH buffer HEPES, 0.1 μM Calcein-AM, and 10 μM propidium iodide (PI). Calcein acetoxymethyl ester (Calcein-AM), a cell-permeant dye, was used to determine cell viability both before and after the photodynamic treatment. In live cells the nonfluorescent Calcein-AM is converted to a green-fluorescent Calcein, after acetoxymethyl ester hydrolysis by intracellular esterases. Meanwhile, PI marks the nuclei once the integrity of the cell membrane is compromised, that is, detecting dead or dying cells. After 1 h incubation in the dark at 37 °C, the cells were replaced with fresh media and exposed to light at a dose rate of 3.2 mW/cm^2 at various light doses. The dye laser excited by an argon ion laser was tuned to emit the drug-activating wavelength, 647 nm. Following illumination, the cell images were acquired with a Perkin-Elmer UltraView confocal microscope system equipped with an argon−krypton laser. Pre-exposure images were taken with an oil immersion 60× objective lens in two channels (488 nm excitation of the Calcein converted from Calcein-AM, and 568 nm excitation of the PI). Images were taken every two minutes, for up to 2 h, to monitor cell death. Finally, a 20× objective was used to broaden the field of view and allow concurrent comparison of the cells exposed to light along with those that had not been exposed.

The cells were first washed with buffer and then fresh DMEM medium was added. Calcein, PI, and F3-Cys targeted PEGylated CD linked HPPH conjugated AFPAA NPs were added into the cell medium. After 15 min incubation, the NP residues were removed by using fresh DMEM media, followed by illumination at 647 nm, and monitored thereafter.

Conflict of Interest: The authors declare no competing financial interest.

Acknowledgment. This work has been supported by NIH/NCI R33CA125297 (R. Kopelman) and RO1 CA127369 (R. Pandey and R. Kopelman). The Electron Microbeam Analysis Laboratory at the University of Michigan is also gratefully acknowledged for the use of the SEM.

Supporting Information Available: Particle size distribution by DLS and spectra of singlet oxygen measurement. This material is available free of charge *via* the Internet at http://pubs.acs.org.

REFERENCES AND NOTES

1. Brannon-Peppas, L.; Blanchette, J. O. Nanoparticle and Targeted Systems for Cancer Therapy. *Adv. Drug. Deliver. Rev.* **2004**, *56*, 1649–1659.
2. Sathornsumetee, S.; Reardon, D. A.; Desjardins, A.; Quinn, J. A.; Vredenburgh, J. J.; Rich, J. N. Molecularly Targeted Therapy for Malignant Glioma. *Cancer* **2007**, *110*, 13–24.
3. Orringer, D. A.; Koo, Y. E. L.; Chen, T.; Kim, G.; Hah, H. J.; Xu, H.; Wang, S. Y.; Keep, R.; Philbert, M. A.; Kopelman, R.; *et al*. *In Vitro* Characterization of a Targeted, Dye-Loaded Nanodevice for Intraoperative Tumor Delineation. *Neurosurgery* **2009**, *64*, 965–971.
4. Gutman, R. L.; Peacock, G.; Lu, D. R. Targeted Drug Delivery for Brain Cancer Treatment. *J. Controlled Release* **2000**, *65*, 31–41.
5. Szakacs, G.; Paterson, J. K.; Ludwig, J. A.; Booth-Genthe, C.; Gottesman, M. M. Targeting Multidrug Resistance in Cancer. *Nat. Rev. Drug. Discovery* **2006**, *5*, 219–234.
6. Wagnieres, G. A.; Star, W. M.; Wilson, B. C. *In Vivo* Fluorescence Spectroscopy and Imaging for Oncological Applications. *Photochem. Photobiol.* **1998**, *68*, 603–632.
7. Moore, G. E.; Peyton, W. T.; French, L. A.; Walker, W. W. The Clinical Use of Fluorescein in Neurosurgery—The Localization of Brain Tumors. *J. Neurosurg.* **1948**, *5*, 392–398.
8. Nie, G.; Hah, H. J.; Kim, G.; Lee, Y.-E. K.; Qin, M.; Ratani, T. S.; Fotiadis, P.; Miller, A.; Kochi, A.; Gao, D.; *et al*. Targeted Hydrogel Nanoparticles with Covalently Linked Coomassie Blue for Brain Tumor Delineation Visible to the Surgeon's Eyes. *Small* **2012**, 10.1002/smll.201101607.
9. Ferrari, M. Cancer Nanotechnology: Opportunities and Challenges. *Nat. Rev. Cancer* **2005**, *5*, 161–171.
10. Barolet, D. Light-Emitting Diodes (LEDs) in Dermatology. *Semin. Cutaneous Med. Surg.* **2008**, *27*, 227–238.
11. Kanu, O. O.; Mehta, A.; Di, C. H.; Lin, N. J.; Bortoff, K.; Bigner, D. D.; Yan, H.; Adamson, D. C. Glioblastoma Multiforme: A Review of Therapeutic Targets. *Expert. Opin. Ther. Targets* **2009**, *13*, 701–718.
12. Kostron, H.; Fiegelea, T.; Akatunaa, E. Combination of FOSCAN Mediated Fluorescence Guided Resection and Photodynamic Treatment as New Therapeutic Concept for Malignant Brain Tumors. *Med. Laser. Appl.* **2006**, *21*, 285–290.
13. Stummer, W.; Novotny, A.; Stepp, H.; Goetz, C.; Bise, K.; Reulen, H. J. Fluorescence-Guided Resection of Glioblastoma Multiforme Utilizing 5-ALA-Induced Porphyrins: A Prospective Study in 52 Consecutive Patients. *J. Neurosurg.* **2000**, *93*, 1003–1013.
14. Kim, J.; Park, S.; Lee, J. E.; Jin, S. M.; Lee, J. H.; Lee, I. S.; Yang, I.; Kim, J. S.; Kim, S. K.; Cho, M. H.; *et al*. Designed Fabrication of Multifunctional Magnetic Gold Nanoshells and Their Application to Magnetic Resonance Imaging and Photothermal Therapy. *Angew. Chem., Int. Ed.* **2006**, *45*, 7754–7758.
15. Fonseca, C.; Simoes, S.; Gaspar, R. E. Paclitaxel-Loaded PLGA Nanoparticles: Preparation, Physicochemical Characterization and *in Vitro* Anti-Tumoral Activity. *J. Controlled Release* **2002**, *83*, 273–286.
16. Lee, A. L. Z.; Wang, Y.; Cheng, H. Y.; Pervaiz, S.; Yang, Y. Y. The Co-delivery of Paclitaxel and Herceptin Using Cationic Micellar Nanoparticles. *Biomaterials* **2009**, *30*, 919–927.
17. Husseini, G. A.; Pitt, W. G. Micelles and Nanoparticles for Ultrasonic Drug and Gene Delivery. *Adv. Drug. Delivery Rev.* **2008**, *60*, 1137–1152.
18. Koo, Y. E. L.; Reddy, G. R.; Bhojani, M.; Schneider, R.; Philbert, M. A.; Rehemtulla, A.; Ross, B. D.; Kopelman, R. Brain Cancer Diagnosis and Therapy with Nanoplatforms. *Adv. Drug. Delivery Rev.* **2006**, *58*, 1556–1577.
19. Gupta, A.; Wang, S.; Pera, P.; Rao, K. V. R.; Patel, N.; Ohulchanskyy, T. Y.; Missert, J.; Morgan, J.; Koo-Lee, Y.-E.; Kopelman, R.; *et al*., Multifunctional Nanoplatforms for Fluorescence Imaging and Photodynamic Therapy Developed by Post-Loading Photosensitizer and Fluorophore to Polyacrylamide Nanoparticles. *Nanomed.-Nanotechnol.* 2011, DOI: 10.1016/j.nano.2011.11.011.
20. Park, I. K.; Ng, C. P.; Wang, J.; Chu, B.; Yuan, C.; Zhang, S.; Pun, S. H. Determination of Nanoparticle Vehicle Unpackaging by MR Imaging of a T-2 Magnetic Relaxation Switch. *Biomaterials* **2008**, *29*, 724–732.
21. Wang, Y.; Gao, S. J.; Ye, W. H.; Yoon, H. S.; Yang, Y. Y. Co-delivery of Drugs and DNA from Cationic Core−Shell

Nanoparticles Self-Assembled from a Biodegradable Copolymer. *Nat. Mater.* **2006**, *5*, 791–796.
22. Akagi, T.; Baba, M.; Akashi, M. Preparation of Nanoparticles by the Self-Organization of Polymers Consisting of Hydrophobic and Hydrophilic Segments: Potential Applications. *Polymer* **2007**, *48*, 6729–6747.
23. Kim, J.; Kim, H. S.; Lee, N.; Kim, T.; Kim, H.; Yu, T.; Song, I. C.; Moon, W. K.; Hyeon, T. Multifunctional Uniform Nanoparticles Composed of a Magnetite Nanocrystal Core and a Mesoporous Silica Shell for Magnetic Resonance and Fluorescence Imaging and for Drug Delivery. *Angew. Chem., Int. Ed.* **2008**, *47*, 8438–8441.
24. Weng, K. C.; Noble, C. O.; Papahadjopoulos-Sternberg, B.; Chen, F. F.; Drummond, D. C.; Kirpotin, D. B.; Wang, D. H.; Hom, Y. K.; Hann, B.; Park, J. W. Targeted Tumor Cell Internalization and Imaging of Multifunctional Quantum Dot-Conjugated Immunoliposomes *in Vitro* and *in Vivo*. *Nano Lett.* **2008**, *8*, 2851–2857.
25. Lee, Y.-E. K.; Kopelman, R., Targeted Hydrogel Nanoparticles for Imaging, Surgery and Therapy of Cancer. In *Multifunctional Nanoparticles for Drug Delivery: Imaging, Targeting and Delivery*; Prud'homme, R. K., Svenson, S., Eds.; Springer Science+Business Media, LLC.; New York, 2012; pp 225−256.
26. Winer, I.; Wang, S.; Lee, Y.-E. K.; Fan, W.; Gong, Y.; Burgos-Ojeda, D.; Spahlinger, G.; Kopelman, R.; Buckanovich, R. J. F3 Targeted Cisplatin/Hydrogel Nanoparticles as an Effective Therapeutic which Targets Both Murine and Human Ovarian Tumor Endothelial Cells *in Vivo*. *Cancer. Res.* **2011**, *71*, 289.
27. Zimmermann, A.; Ritsch-Marte, M.; Kostron, H. mTHPC-Mediated Photodynamic Diagnosis of Malignant Brain Tumors. *Photochem. Photobiol.* **2001**, *74*, 611–616.
28. Moan, J.; Berg, K. The Photodegradation of Porphyrins in Cells Can Be Used To Estimate the Lifetime of Singlet Oxygen. *Photochem. Photobiol.* **1991**, *53*, 549–553.
29. Haley, B.; Frenkel, E. Nanoparticles for Drug Delivery in Cancer Treatment. *Urol. Oncol.: Semin. Orig. Invest.* **2008**, *26*, 57–64.
30. Tang, W.; Xu, H.; Kopelman, R.; Philbert, M. A. Photodynamic Characterization and *in Vitro* Application of Methylene Blue-Containing Nanoparticle Platforms. *Photochem. Photobiol.* **2005**, *81*, 242–249.
31. Bellnier, D. A.; Greco, W. R.; Nava, H.; Loewen, G. M.; Oseroff, A. R.; Dougherty, T. J. Mild Skin Photosensitivity in Cancer Patients Following Injection of Photochlor (2-[1-Hexyloxyethyl]-2-Devinyl Pyropheophorbide-a; HPPH) for Photodynamic Therapy. *Cancer. Chemoth. Pharm.* **2006**, *57*, 40–45.
32. Wang, S.; Fan, W.; Kim, G.; Hah, H. J.; Lee, Y.-E. K.; Kopelman, R.; Ethirajan, M.; Gupta, A.; Goswami, L. N.; Pera, P.; *et al.* Novel Methods to Incorporate Photosensitizers into Nanocarriers for Cancer Treatment by Photodynamic Therapy. *Laser. Surg. Med.* **2011**, *43*, 686–695.
33. Wang, Z.; Chui, W. K.; Ho, P. C. Design of a Multifunctional PLGA Nanoparticulate Drug Delivery System: Evaluation of Its Physicochemical Properties and Anticancer Activity to Malignant Cancer Cells. *Pharm. Res.* **2009**, *26*, 1162–1171.
34. Christian, S.; Pilch, J.; Akerman, M. E.; Porkka, K.; Laakkonen, P.; Ruoslahti, E. Nucleolin Expressed at the Cell Surface Is a Marker of Endothelial Cells in Angiogenic Blood Vessels. *J. Cell. Biol.* **2003**, *163*, 871–878.
35. Yu, W. Y.; Zhang, N. Surface Modification of Nanocarriers for Cancer Therapy. *Curr. Nanosci.* **2009**, *5*, 123–134.
36. Byrne, J. D.; Betancourt, T.; Brannon-Peppas, L. Active Targeting Schemes for Nanoparticle Systems in Cancer Therapeutics. *Adv. Drug. Delivery Rev.* **2008**, *60*, 1615–1626.
37. Yoshida, M.; Roh, K. H.; Lahann, J. Short-Term Biocompatibility of Biphasic Nanocolloids with Potential Use as Anisotropic Imaging Probes. *Biomaterials* **2007**, *28*, 2446–2456.
38. Kopelman, R.; Koo, Y. E. L.; Philbert, M.; Moffat, B. A.; Reddy, G. R.; McConville, P.; Hall, D. E.; Chenevert, T. L.; Bhojani, M. S.; Buck, S. M.; *et al.* Multifunctional Nanoparticle Platforms for *in Vivo* MRI Enhancement and Photodynamic Therapy of a Rat Brain Cancer. *J. Magn. Magn. Mater.* **2005**, *293*, 404–410.
39. Zhang, Y.; Zhu, W.; Wang, B. B.; Ding, J. D. A Novel Microgel and Associated Post-Fabrication Encapsulation Technique of Proteins. *J. Controlled Release* **2005**, *105*, 260–268.
40. Tan, Y.; Xu, C. S.; Xia, X. S.; Yu, H. P.; Bai, D. Q.; He, Y.; Xu, J.; Wang, P.; Wang, X. N.; Leung, A. W. N. Preliminary Studies on LED-Activated Pyropheophorbide-Alpha Methyl Ester Killing Cisplatin-Resistant Ovarian Carcinoma Cells. *Laser. Phys.* **2009**, *19*, 1045–1049.
41. Chiu, H. C.; Lin, Y. F.; Hung, S. H. Equilibrium Swelling of Copolymerized Acrylic Acid- Methacrylated Dextran Networks: Effects of pH and Neutral Salt. *Macromolecules* **2002**, *35*, 5235–5242.
42. Holland, S. J.; Tighe, B. J.; Gould, P. L. Polymers for Biodegradable Medical Devices. 1. The Potential of Polyesters as Controlled Macromolecular Release Systems. *J. Controlled Release* **1986**, *4*, 155–180.
43. Torchilin, V. P. Multifunctional Nanocarriers. *Adv. Drug. Delivery Rev.* **2006**, *58*, 1532–1555.
44. Liu, Y. Y.; Miyoshi, H.; Nakamura, M. Nanomedicine for Drug Delivery and Imaging: A Promising Avenue for Cancer Therapy and Diagnosis Using Targeted Functional Nanoparticles. *Int. J. Cancer.* **2007**, *120*, 2527–2537.
45. Porkka, K.; Laakkonen, P.; Hoffman, J. A.; Bernasconi, M.; Ruoslahti, E. A Fragment of the HMGN2 Protein Homes to the Nuclei of Tumor Cells and Tumor Endothelial Cells *in Vivo*. *Proc. Natl. Acad. Sci. U.S.A.* **2002**, *99*, 7444–7449.
46. Tang, W.; Xu, H.; Park, E. J.; Philbert, M. A.; Kopelman, R. Encapsulation of Methylene Blue in Polyacrylamide Nanoparticle Platforms Protects Its Photodynamic Effectiveness. *Biochem. Biophys. Res. Commun.* **2008**, *369*, 579–583.
47. Gao, D.; Agayan, R. R.; Xu, H.; Philbert, M. A.; Kopelman, R. Nanoparticles for Two-Photon Photodynamic Therapy in Living Cells. *Nano Lett.* **2006**, *6*, 2383–2386.
48. Gao, D.; Xu, H.; Philbert, M. A.; Kopelman, R. Ultrafine Hydrogel Nanoparticles: Synthetic Approach and Therapeutic Application in Living Cells. *Angew. Chem., Int. Ed.* **2007**, *46*, 2224–2227.
49. Gao, D.; Xu, H.; Philbert, M. A.; Kopelman, R. Bioeliminable Nanohydrogels for Drug Delivery. *Nano Lett.* **2008**, *8*, 3320–3324.
50. Cheng, Y.; Samia, A. C.; Meyers, J. D.; Panagopoulos, I.; Fei, B. W.; Burda, C. Highly Efficient Drug Delivery with Gold Nanoparticle Vectors for *in Vivo* Photodynamic Therapy of Cancer. *J. Am. Chem. Soc.* **2008**, *130*, 10643–10647.
51. Baba, K.; Pudavar, H. E.; Roy, I.; Ohulchanskyy, T. Y.; Chen, Y. H.; Pandey, R. K.; Prasad, P. N. New Method for Delivering a Hydrophobic Drug for Photodynamic Therapy Using Pure Nanocrystal Form of the Drug. *Mol. Pharmaceutics* **2007**, *4*, 289–297.
52. Grabarek, Z.; Gergely, J. Zero-Length Crosslinking Procedure with the Use of Active Esters. *Anal. Biochem.* **1990**, *185*, 131–135.
53. Staros, J. V.; Wright, R. W.; Swingle, D. M. Enhancement by *N*-Hydroxysulfosuccinimide of Water-Soluble Carbodiimide-Mediated Coupling Reactions. *Anal. Biochem.* **1986**, *156*, 220–222.
54. Veiseh, O.; Sun, C.; Gunn, J.; Kohler, N.; Gabikian, P.; Lee, D.; Bhattarai, N.; Ellenbogen, R.; Sze, R.; Hallahan, A.; *et al.* Optical and MRI Multifunctional Nanoprobe for Targeting Gliomas. *Nano Lett.* **2005**, *5*, 1003–1008.